www.czasopisma.pan.pl PAN POLSKA AKADEMIA NAUK www.journals.pan.pl

Arch. Min. Sci. **68** (2023), 2, 301-318

Electronic version (in color) of this paper is available: http://mining.archives.pl

DOI: https://doi.org/10.24425/ams.2023.146181

SHUANG LIANG[1,2,3*], DI WANG[1,2], DAN LIU[4], YANG TIAN[3], HAIBO WANG[1,2], FENGXIA LI[1,2], GANG DONG[5], CHENGFENG YIN[6], YI YANG[7]

FRACTURE INTERFERENCE AND PROPAGATION GEOMETRY OF HYDRAULIC FRACTURES BASED ON XFEM IN AN UNCONVENTIONAL OIL RESERVOIR

Unconventional oil and gas reservoirs are characterised by low porosity, low permeability and low natural deliverability. At present, horizontal wells staged fracturing is an effective development method. However, in the case of staged hydraulic fracturing in horizontal wells, stress interference occurs between multiple fractures, leading to fracture deformation and even inhibiting the formation of fractures, thereby affecting reservoir production. In this paper, based on the extended finite element method (XFEM), considering the fluid flow in the fracture and fracturing fluid filtration, we analyse the effects of fracturing fluid pumping rate, fracture spacing and elastic modulus on horizontal in-situ stress, fracture parameters and fracture extension pattern during different fracturing initiation processes. The results show that the induced stress generated by the action of fracturing fluid changes the direction of horizontal in-situ stress in the elliptical region around the fracture. In the mode of simultaneous fracture initiation (TFIS), the extension of two symmetrical fractures is "repulsive"; in the mode of two fractures initiated at different times (TFIDT), the extension direction is "mutual attraction". A large pumping rate and small elastic modulus are conducive to fracture propagation. In the TFIS mode, two fractures alternately expand, while in the TFIDT mode, the impact of rock mechanical properties and construction parameters on fracture propagation will be amplified. The extension of subsequent fractures will be restrained, especially when the fracture spacing is less than 10 m. The width of the previously created fracture will be severely affected, even causing a partial closure and becoming elongated fractures.

Keywords: hydraulic fracturing; fracture interference; XFEM; fracture propagation geometry; unconventional oil reservoir

[1] STATE KEY LABORATORY OF SHALE OIL AND GAS ENRICHMENT MECHANISMS AND EFFECTIVE DEVELOPMENT, BEIJING, CHINA
[2] STATE ENERGY CENTER FOR SHALE OIL RESEARCH AND DEVELOPMENT, BEIJING, CHINA
[3] DEPARTMENT OF PETROLEUM ENGINEERING, NORTHEAST PETROLEUM UNIVERSITY, DAQING CHINA
[4] PIPECHINA OIL & GAS PIPELINE CONTROL CENTER, BEIJING, 122000, CHINA
[5] THE EIGHTH OIL PRODUCTION PLANT OF DAQING OILFIELD LIMITED COMPANY, DAQING CHINA
[6] THE FOURTH OIL PRODUCTION PLANT OF DAQING OILFIELD LIMITED COMPANY, DAQING CHINA
[7] THE TENTH OIL PRODUCTION PLANT OF DAQING OILFIELD LIMITED COMPANY, DAQING CHINA

* Corresponding author: liangshuang21@163.com

1. Introduction

With the rapid development of the economy, energy demand has increased sharply, making the contradiction between supply and demand more prominent. Unconventional oil and gas resources have gradually entered the view of scientists owing to their sizable resources [10]. However, it is difficult to achieve economic and effective utilisation using conventional development technologies, owing to their low porosity-low permeability and low natural deliverability. The key to the efficient development of unconventional oil and gas is currently horizontal well multi-fracturing technology [1,9,12,17]. Several studies confirmed that unlike the symmetrical double fractures in vertical hydraulic fracturing, staged hydraulic fracturing tends to form complex fracture networks that include multiple fractures, resulting in greater reservoir volume and ultimately, higher production. However, in the case of staged hydraulic fracturing in horizontal wells, there is often stress interference between multiple fractures. Interference between fractures can cause deformation and deflection, and even inhibit fracture generation, affecting the effectiveness of reservoir volume improvement and ultimately impacting reservoir production [24]. Consequently, investigating fracture interference and propagation geometry of horizontal well multi-fracturing is crucial.

Scholars' research on fracture interference and propagation is mainly based on laboratory physical experiments [13,26], analytical models and numerical models [18,20,22]. Among them, the extended finite element method (XFEM), which combines the finite element theory with fracture mechanics theory, has gradually received increasing attention because fracture can extend along any path and solve cracking problems with a minimal grid. The method introduces a novel enriched function to model discontinuities in the displacement field caused by cracks, which can be achieved by introducing additional terms related to the enriched degrees of freedom without any re-meshing process during a crack propagation [5,15,21,26]. Chen et al. [27]studied the extension model using xFEM, and verified the accuracy of this method. Zeng et al. [14]solved the crack flow and the rock stress fields using FEM and xFEM and verified the correctness of xFEM in hydraulic fracturing. Youn et al. [4], Sepehri et al. [6] and Haddad et al. [9] established three-dimensional hydraulic fracturing models through the XFEM method to analyse the propagation law of hydraulic fractures in unconventional reservoirs. Sepehri et al. [6] and Wang et al. [23] conducted the influence of perforation parameters and rock anisotropy on fracture propagation. Sandeep et al. [16] combined xFEM with the freedom degree of pore pressure to simulate various boundary issues related to hydraulic fracturing in permeable media and studied the effect of geomechanical properties and construction parameters on hydraulic fracturing. Zhou et al. [18] established a three-dimensional fracturing fracture propagation model through indoor physical experiments and discrete element methods. They confirmed that bedding is one of the important factors causing the anisotropy of shale mechanical properties, and studied the fracture propagation patterns under different bedding strengths and fracturing engineering parameters. Zhang et al. [25] compared commonly used fracturing simulation methods and analysed the impact of construction sequence on fracture morphology using XFEM. Rossana et al. [3] established a semicircular bending test model based on XFEM, explored the formation and propagation of cracks in the rock, and proposed a novel analytical formula to solve the response of materials in terms of load crack mouth opening displacement. However, it is not entirely understood about stress changes and interference between fractures in the process of dynamic propagation for multiple fractures, especially fracture propagation under different initiation modes. This paper analyses the stress changes between fractures in different initiation modes and their effects on fracture morphology based on the XFEM method, considering fluid flow and fracturing fluid filtration in the fractures.

2. Model description

2.1. The criterion of XFEM

For XFEM, the discontinuity of displacement is represented by the extension function associated with the additional degrees of freedom so that the fracture propagation path is not constrained by the mesh. The function of the displacement vector is as follows:

$$u(x)=\sum_{i=1}^{m}N_i(x)\left(u_i+H(X)a_i+\sum_{j=1}^{4}F_j(x)b_i^j\right) \tag{1}$$

Where m is the finite element node; $N_i(x)$ is the displacement function of an ordinary node; u_i is the displacement vector of a usual node; $H(X)$ is the discontinuous jump function of the crack surface; a_i, b_i is the extended degree of freedom vector for the node; $F_j(x)$ is the asymptotic function of the stress at the crack tip.

The maximum principal stress criterion is adopted in this model, the function is as follows:

$$f=\left\{\frac{\langle\sigma_{\max}\rangle}{\sigma'_{\max}}\right\} \tag{2}$$

Where $\sigma_{\max}$ is the maximum principal stress, MPa; $\sigma'_{\max}$ is the maximum allowable principal stress, MPa; $\langle\cdot\rangle$ is the Macaulay parenthesis.

The BK criterion [11] is used for the damage evolution process after fracture initiation, as follows:

$$G_{equiv,n}=G_{IC}+(G_{IIC}-G_{IC})\left(\frac{G_{III}+G_{II}}{G_{III}+G_{II}+G_I}\right)^{\eta} \tag{3}$$

Where $G_{equiv,n}$ is the critical fracture energy release rate, N/mm; G_{IC}, G_{IIC} are fracture toughness for Type I and Type II, respectively, N/mm; G_I, G_{II}, G_{III} are the fracture energy release rates of normal, first tangential and second tangential respectively, N/mm; η is the work done by each stress in the corresponding displacement direction, J.

2.2. Rock deformation equation

It is universally acknowledged that rock deformation occurs during fracturing. The solid equilibrium equation of rock can be obtained using the principle of virtual work, as shown in Eq. (4):

$$\int_V\sigma\delta\varepsilon dV=\int_S t^b\delta v dS+\int_V F\delta v dV \tag{4}$$

Where V is the unit volume, m^3; σ is the total stress of matrix, Pa; $\delta\varepsilon$ is the virtual strain rate, s^{-1}; F is the volumetric force, N/m^3; δv is the virtual velocity, m/s; S is the unit area, m^2; t^b is the external surface force per unit area, N/m^2.

2.3. Flow equation

The fluid is assumed to be an incompressible Newton fluid, and fluid filtration is not considered. The continuity equation can be expressed by Eq. (5):

$$\frac{d}{dt}\left(\int_{\Omega}\rho_w\phi d\Omega\right)=-\int_{S}\rho_w\phi n v_w dS \tag{5}$$

Where Ω is the integral space, m^3; S is the space of integral surface, m^2; ρ_w is the fluid density, kg/m^3; ϕ is porosity; n is the normal direction of the fracture external surface; v_w is the flow velocity, m/s.

Since Eq. (5) conforms to Darcy law:

$$v_w=-\frac{1}{\phi g\rho_w}K\left(\nabla p_w-\rho_w g\right) \tag{6}$$

Where g is the gravitational acceleration, m/s^2; ∇p_w is the pressure gradient, Pa; K is the matrix permeability, m^2.

The fluid-solid coupling equation can be derived from Eq. (1) to Eq. (6).

2.4. Model setup and verification

A two-dimensional formation model with a dimension of 50 m × 50 m is established according to X Block in Jiangsu Oilfield. As shown in Fig. 1, the boundary pressure is constant, and the formation is isotropic without natural fractures. The X direction is the horizontal minimum principal stress direction; the Y direction is the maximum horizontal in-situ stress direction, and the vertical in-situ stress is loaded perpendicular to the plane direction. For a single fracture model, the injection point is in the centre of the model, and the pre-existing perforated area is the initial fracture; for the dual fractures model, the injection points are symmetrically distributed in the centre of the model, and the pre-existing fractures are the same as above. The parameters of the calculation model are shown in Table 1.

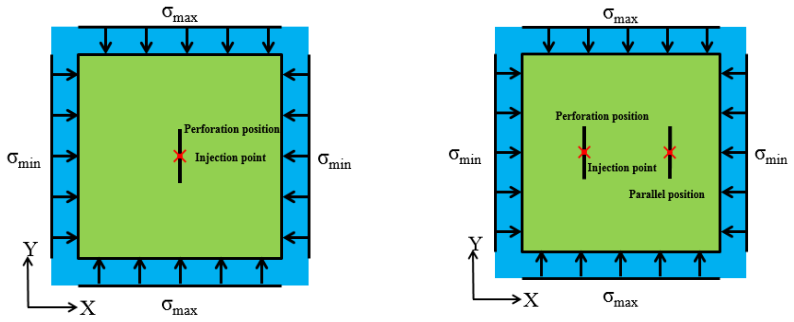

(a) single crack (b) two cracks

Fig. 1. Schematic of Model

TABLE 1

The parameter of model

Parameters	Value	Parameters	Value
Model size/m	50×50	Viscosity of fracturing fluid /mPa·s	1
Elastic modulus/GPa	25	Pumping rate of fracturing fluid /$m^3 \cdot min^{-1}$	6
Poisson's ratio	0.2	Initial pore pressure /MPa	40
Tensile strength/MPa	2	Maximum horizontal principal stresses/MPa	90
Permeability/10^{-3} μm^2	2	Minimum horizontal principal stresses/MPa	83
Filtration coefficient/10^{-14} m/Pa·s	1	Vertical principal stress/MPa	73

In order to validate XFEM simulation results, we established a two-dimensional fracture propagation model containing three parallel cracks. The results of the XFEM method and laboratory experiment [2] are shown in Fig. 2. When the fracture spacing is 30 mm, the propagation of the intermediate fracture is constrained by the fractures on both sides, resulting in a shorter propagation distance. Meanwhile, the fractures on both sides are "mutually repulsive" due to the interference between fractures. Hence, the fracture trajectories simulated by the XFEM method verify the laboratory results.

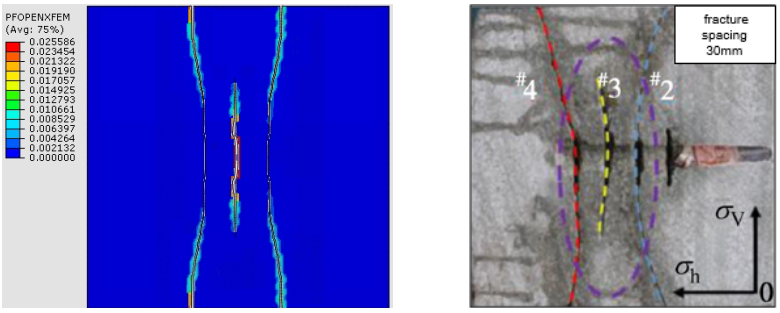

(a) XFEM (b) laboratory experiment

Fig. 2. Comparison of fracture geometry between XFEM and laboratory experiment

3. Result and analysis

3.1. Influence of in-situ stress on fracture interference

3.1.1. Stress shadow effects

Fig. 3 shows the propagation pattern of two parallel fractures with a 5 m spacing, and the fractures gradually extend as the injection time increases. Taking the borehole as the axis, the stress field around the fracture and the deformation of the fracture are symmetrically distributed, and the maximum and minimum principal stresses fluctuate violently, resulting in multiple stress fields that inevitably affect the propagation of the fracture. The most obvious is that the fracture propagation near the injection point is suppressed, with a wide middle and narrow end, and the tip deflects under stress interference.

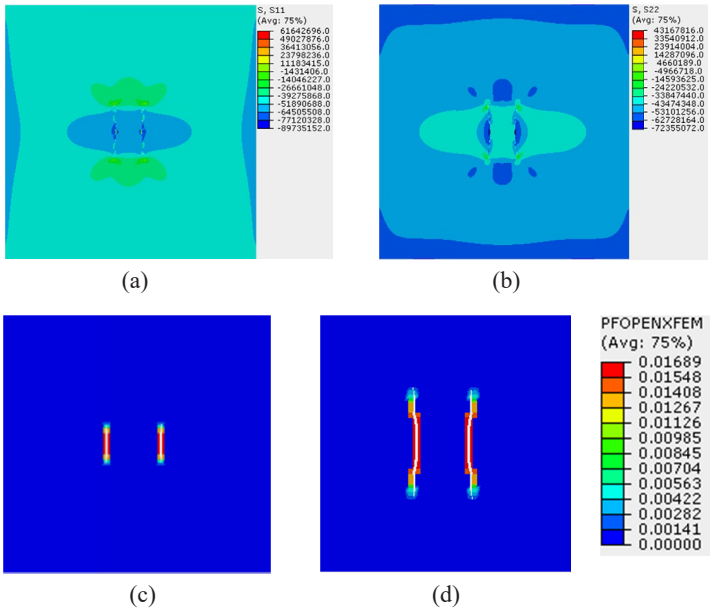

Fig. 3. Stress shadow distribution and Fracture width variation of parallel fractures (a) minimum horizontal principal stresses; (b) maximum horizontal principal stresses; (c) fracture width at 2.5s; (d) fracture width at 5.0s

3.1.2. The influence of horizontal stress bias on fracture interference

When there is only one fracture, the horizontal stress bias increases, the fracture length increases, and the width decreases. As shown in Table 2 and Fig. 4, for two fractures, when the horizontal stress bias is 4 MPa or 7 MPa, the propagation and opening law of the cracks are the same as those of a single crack. At 10 MPa, the two fractures maintain the same geometry at the initial stage of fracturing. After extending to a certain length, the extension direction of two symmetrical fractures is “mutually repulsive”. The left fracture width increases, the fracture length changes slightly. In contrast, the width of right fracture decreases rapidly and the fracture length increases rapidly, as shown in Fig. 4(c). This indicates that when the stress bias increases to a certain value, the extension and opening law of the two fractures are different from those of a single fracture. Combined with the analysis results of stress shadow effect as mentioned above, there are multiple stress fields at the tip of the two fractures, and the right fracture

TABLE 2

Fracture length and width under different horizontal stress bias

Single fracture			Two fractures			
Horizontal stress bias/MPa	**Fracture length/m**	**Fracture width/mm**	**Left fracture length/m**	**Left fracture width/mm**	**Right fracture length/m**	**Right fracture width/mm**
4	11	17.52	10	18.12	10	18.12
7	11	17.33	11	17.51	11	17.51
10	12	16.29	10	18.39	13	13.92

is interfered by the left fracture, causing severe changes in the horizontal principal stress around right fracture. The greater the horizontal stress bias, the more obvious the impact on the fracture width, and the right fracture become more "long and narrow".

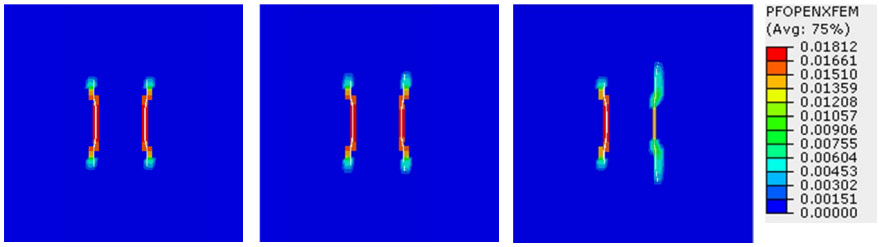

(a) 4 MPa (b) 7 MPa (c) 10 MPa

Fig. 4. Simulation diagram of parallel fracture widths under different horizontal stress bias

3.2. Influence of initiation modes and construction parameters on fracture interference

The development of unconventional oil and gas reservoirs adopts long horizontal section and segmented horizontal well fracturing. The fractures initiated at the same time are referred to as TFIS mode, the fractures initiated at different times are called TFIDT mode. Due to the mutual interference between fractures, different initiation modes have different effects on fracture propagation. This part will discuss the influence of fracturing fluid pumping rate, fracture spacing and elastic modulus on fracture propagation under different fracture initiation modes.

3.2.1. Two fractures initiated simultaneously (TFIS)

The simulation is conducted with initial fracture spacing of 10 m, an injection time is 8s, and the two fractures are initiated at the same time. We appropriately change the influence factors and refer to the values in Table 1 for other factors to analyse the influencing factors of fracture propagation.

(1) The influence of fracturing fluid pumping rate

Fracturing fluid is used for fracture forming and proppant carrying. This is a key component in the hydraulic fracturing process [7]. The pumping rate inevitably affects the fracture morphology. In terms of the model in Fig. 1(b), different pumping rates (3 m^3/min, 6 m^3/min, 9 m^3/min, 12 m^3/min) are designed. The simulation results are given in Figs. 5-7. Fig. 5 illustrates that with the increase in pumping rate, the width and length of fracture increase to a certain extent. When the pumping rate is less than 6 m^3/min, the change tendency of fracture length and width of the two fractures remain consistent. When the pumping rate is larger than 6 m^3/min, the propagation geometries of the left and right fractures gradually tend to be different. The larger the pumping rate, the greater the difference between the two fractures. Fig. 6 shows the fracture width and net pressure curves at a pumping rate of 12 m^3/min. Green represents the left fracture, red represents the right fracture, the solid line represents the net pressure in the fracture, and the dotted line represents the fracture width. It indicates that the change trends of fracture width and net

pressure are the same for each fracture. When the pumping rate is 12 m^3/min, the fluid pressure loading speed increases. With the extension of time, such as after 6S, the injected fluid will increase the net pressure within the fracture, thereby affecting the formation pressure retaining and breakdown effects and exacerbating fracture interference. In Fig. 6, the green dotted line is higher than the red dotted line, and the green solid line is also higher than the red one, indicating that the width of the left fracture increase, the net pressure in the fracture increases, and the right fracture is squeezed, resulting in a decrease in the width of the right fracture and an increase in its length. As the pressure in the left fracture slows down, the pressure in the right fracture increases, and the width of the fracture increases, which in turn squeezes the left fracture. Under the effect of stress interference, the left fracture width decreases, and the length increases. After a certain period of time, the left and right fractures alternately open and extend, as depicted in Fig. 7.

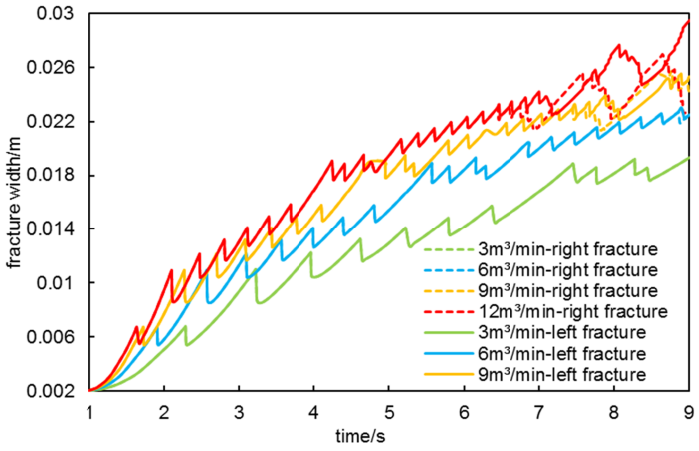

Fig. 5. Fracture width under different pumping rates in TFIS mode

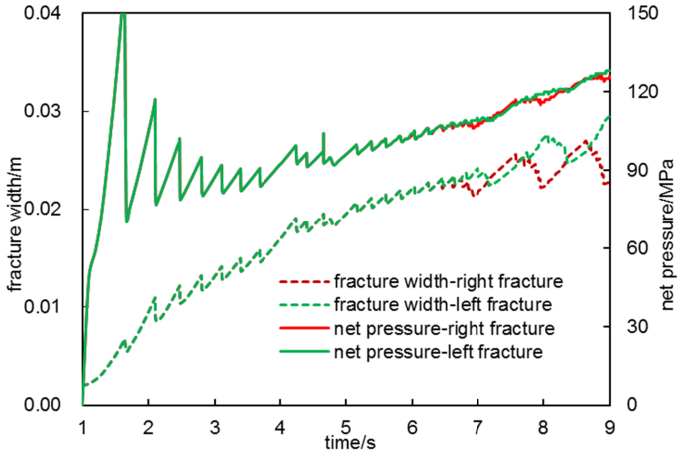

Fig. 6. Fracture width and net pressure at 12m^3/min in TFIS mode

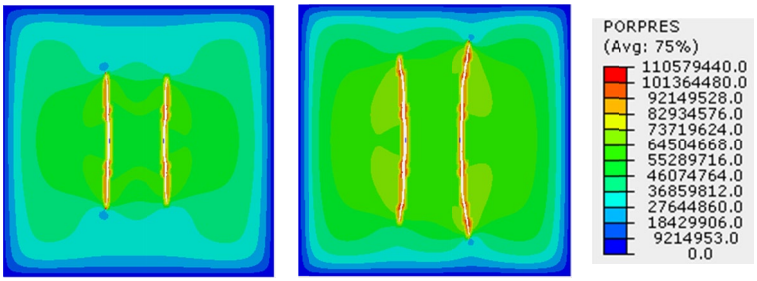

(a) 6.3s (b) 8s

Fig. 7. Pore pressure at different times with a pumping rate 12 m^3/min in TFIS mode

(2) The influence of fracture spacing

If the spacing between two fractures is different, the stress field between the fractures will also be different, which affects the fracture propagation pattern. The fracture propagations under different fracture spacing (5 m, 10 m, 15 m and 20 m) are simulated, and the results are shown in Figs. 8, 9 and Table 3. There are significant differences in the propagation of two fractures under different spacing, especially for the small fracture spacing. In Fig. 8, the fracture width curves with fracture spacing of 15 m and 20 m completely coincide, indicating that when the fracture spacing is relatively far, the stress interference between fractures is small, and the fracture expansion geometry is the same as that of a single fracture. When the fracture spacing is 5 m, the net pressure within the fracture is small and the interference is weak at the initial stage of fracture propagation, and the two fractures extend synchronously along the direction of the maximum principal stress. With the net pressure increases, the two fractures interfere with each other, causing severe fluctuations in the stress field. Following the principle of energy conservation, the fractures near the injection point are strongly constrained, and the inhibition effect of the fracture tip is weakened. The direction of the maximum horizontal principal stresses on both sides of the fracture deflects and appears in an elliptical shape, and the new maximum principal stress zone

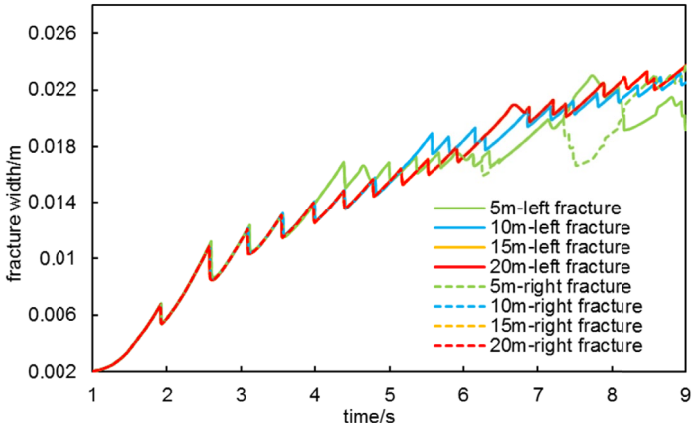

Fig. 8. Fracture width under different fracture spacings in TFIS mode

deviates from the original maximum principal stress direction. The smaller the fracture spacing, the greater the repulsive deflection angle, as depicted in Fig. 9.

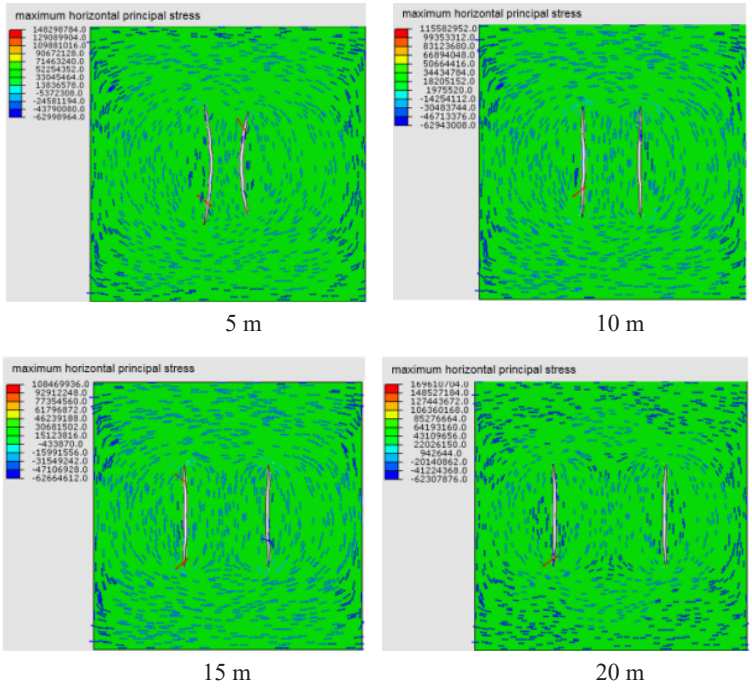

Fig. 9. Maximum horizontal principal stresses with different fracture spacing in TFIS mode

TABLE 3

Fracture length and width under different fracture spacings in TFIS mode

Fracture spacing/m	Left fracture length/m	Left fracture width/mm	Right fracture length/m	Right fracture width/mm
5	20	19.16	19	23.72
10	20	22.53	20	22.53
15	19	23.72	19	23.72
20	19	23.72	19	23.72

(3) The influence of elastic modulus

The elastic modulus is set to 10 GPa, 20 GPa, 30 GPa and 40 GPa respectively, the results are shown in Figs. 10, 11 and Table 4. The elastic modulus increases with the decrease in fracture width. When the elastic modulus is 10 GPa and 20 GPa, the fracture width curves to the left and right fractures overlap. When the elastic modulus is greater than 20 GPa, as the injection time increases, the widths of the two fractures are different. The larger the elastic modulus, the earlier the width gap occurs, and the left and right fractures open alternately, especially when the elastic modulus is 40 GPa, as shown in Fig. 10. According to the results in Table 4, when

the elastic modulus is small, it is easy to form a “short-wide” fracture. As the elastic modulus increases, the two fractures gradually lengthen and narrow, opening alternately with mutual exclusion (Fig. 11), indicating that a larger elastic modulus is conducive to the overall propagation of the fracture. Because elastic modulus can measure the ability to resist elastic deformation, a larger elastic modulus will cause greater elastic deformation stress. That is, a higher brittleness index is conducive to the propagation of fractures.

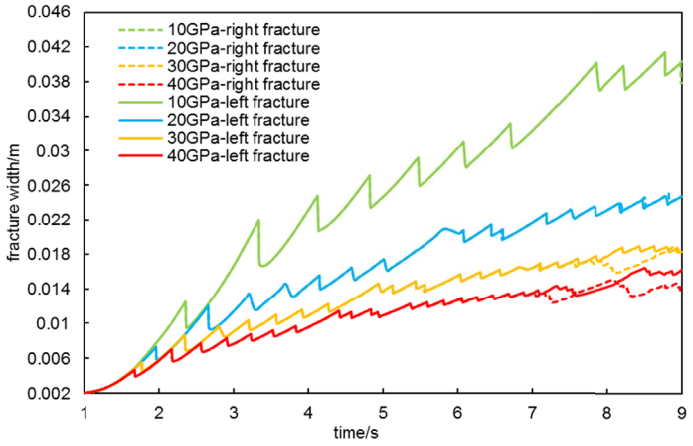

Fig. 10. Fracture width under different elastic modulus in TFIS mode

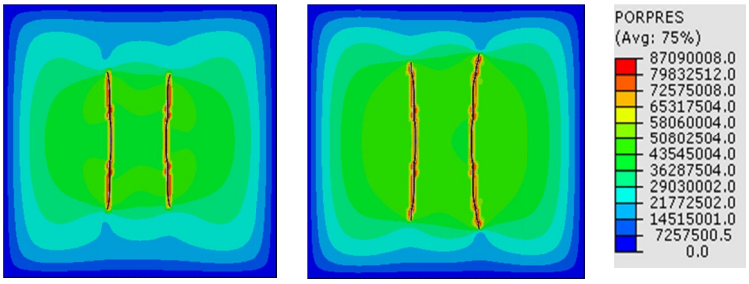

Fig. 11. Pore pressure at different times with an elastic modulus 40 GPa in TFIS mode

TABLE 4

Fracture length and width under different elastic modulus in TFIS mode

Elastic modulus /GPa	Left fracture length/m	Left fracture width/mm	Right fracture length/m	Right fracture width/mm
10	11	40.35	12	37.87
20	18	24.77	18	24.78
30	25	18.29	24	18.73
40	29	16.16	32	13.84

3.2.2. Two fractures initiated at different times (TFIDT)

The initiation process of two fractures in TFIDT mode is as follows: one fracture initiates first after the fracture propagation is completed, pumping is stopped for a period of time, and then the second fracture is initiated. In this part, we adopt the datum in Table 2. The initial fracture spacing is 10 m. The fracturing process can be divided into three stages: fracturing the right fracture for 8s, stopping the pump to hold the pressure for 180s, and then fracturing the left fracture for 8s at the same injection rate.

(1) The influence of fracturing fluid pumping rate

Refer to the first part of 3.2.1 to set the rock and fracture parameters. The simulation results are shown in Figs. 12 and 13. The changes in fracture geometry under different pumping rates mainly occur in the first stage (1-9s) and the third stage (189-197s). In the first stage of TFIDT mode, the right fracture width increases with the injection time, the width and length of the left fracture gradually increase with the increase of injection time in the third stage and the right fracture changes during the propagation of the left fracture. When the pumping rate is 3 m^3/min, the width of the right fracture remains stable (a horizontal line). When the pumping rate is 6 m^3/min, the width of the right fracture performs stepped decline, and the time point of decline is at 195S and 196S. Overall, the change in right fracture width is relatively small. When the pumping rate is less than 6 m^3/min, it is less affected by the "squeezing" of the left fracture expansion. When the pumping rate is more than 6 m^3/min, the influence of stress interference

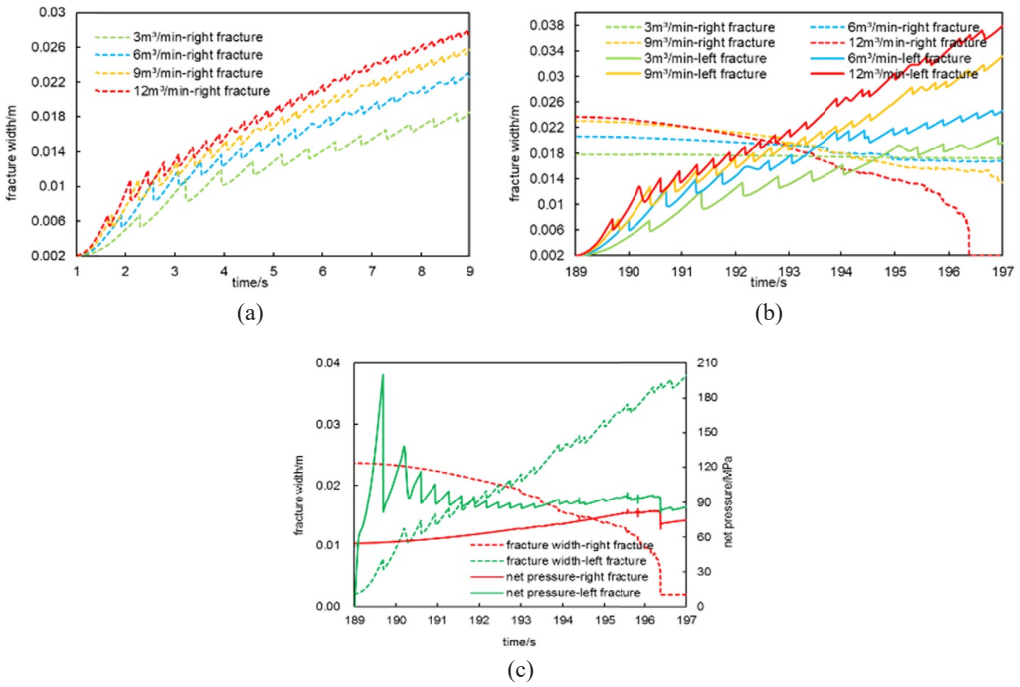

Fig. 12. Fracture width under different pumping rates in TFIDT mode (a) First stage of fracturing; (b) The third stage of fracturing; (c) Fracture width and net pressure at 12 m^3/min

between fractures becomes larger. As the injection time increases, the upper and lower ends of the left fracture deflect to the right, and the right fracture width decreases sharply. Especially at 12 m^3/min, the decrease time of fracture width is earlier than that at 9m^3/min, which means that the larger the pumping rate, the stronger the influence of stress interference, and the fracture width decreases to the preset width. According to the net pressure change (Fig. 12(c)), we can conclude that when the pumping rate is 12 m^3/min, after a certain injection time, the net pressure in the left fracture increases instantaneously, and then gradually declines as the fracture expands, resulting in a "squeezing effect" on the right fracture. Under the influence of stress interference, the width of the right fracture shrinks, and the fracture length increases rapidly, exceeding the left fracture to form a "long-narrow" geometry, as shown in Fig. 13.

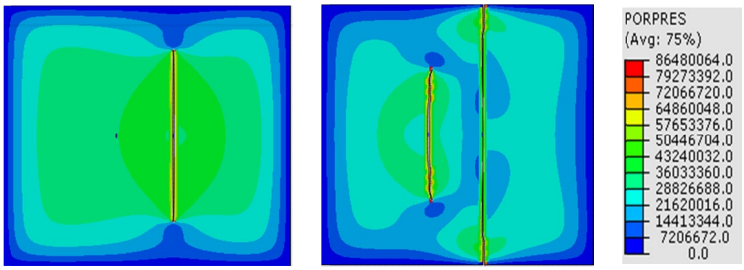

(a) 9s (b) 197s

Fig. 13. Pore pressure at different times with a pumping rate 12 m^3/min in TFIDT mode

(2) The influence of fracture spacing

Refer to 3.2.1 for rock and fracture parameters, and the simulation results are shown in Figs. 14, 15 and Table 5. At the first stage of TFIDF mode, the width of the right fracture increases with the increase of injection time. The width curves of the previously created fracture verify each other, indicating that the previously created fracture is not affected by the spacing (Fig. 14). However, in the third stage of TFIDF mode, with the increase of injection time, the width and length of the left fracture gradually increase, while the width of the right fracture decreases, especially when the fracture spacing is 5 m. As depicted in Fig. 15, when the fracture spacing is 5 m, the right fracture is squeezed, the fracture near the wellbores is partially closed, and a large amount of fluid in the fracture flows into both ends of the fracture so that the right fracture continues to extend. Due to the closure property of the right fracture, the width of the left fracture near wellbores is wider, and the length of the fracture is shorter than that of a single fracture. The fracture deflects to the right under the influence of the maximum horizontal stress, and the two fractures perform inter-attracting. As seen in Table 5, the larger the fracture spacing, the larger the right fracture width, and the smaller the left fracture width changes. When the fracture spacing increases from 5 m to 10 m, the fracture width increases from 10.72 mm to 16.79 mm, and then the spacing continues to increase, with little change in fracture width. When the fracture spacing increases from 15 m to 20 m, the fracture width increases by 1.5 mm. It reveals that when the spacing is small, the right fracture will be squeezed by the stress from the left, leading to a significant reduction in the width of the fracture and a significant increase in its length, forming a "long-narrow" fracture. The greater the spacing, the smaller the fracture interference, which is consistent with the influence law of fracture spacing in TFIS mode.

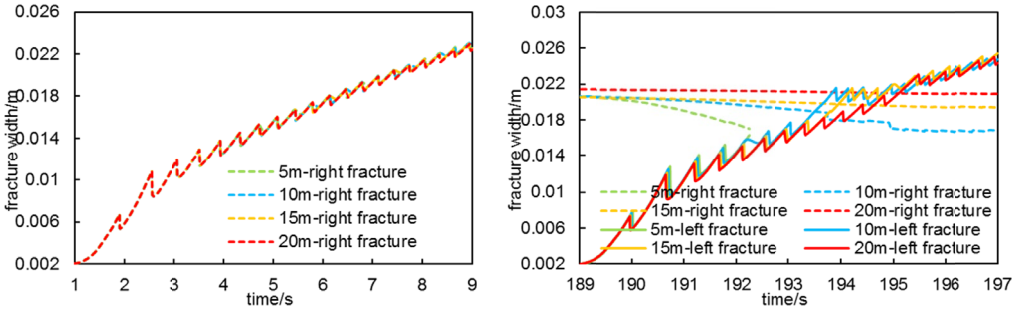

(a) First stage of fracturing (b) The third stage of fracturing

Fig. 14. Fracture width under different fracture spacing in TFIDT mode

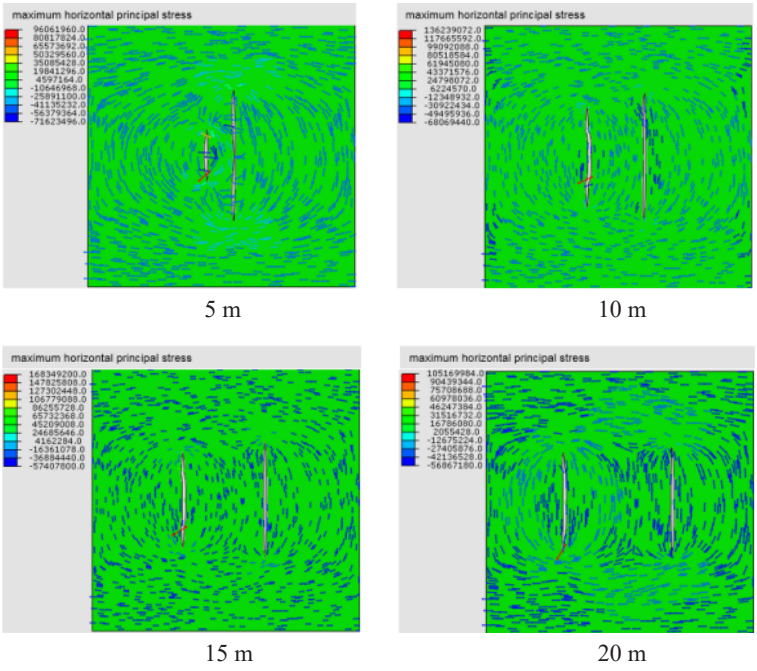

5 m 10 m

15 m 20 m

Fig. 15. Maximum horizontal principal stresses with different fracture spacing in TFIDT mode

TABLE 5

Fracture length and width under different fracture spacings in TFIDT mode

Fracture spacing/m	Left fracture length/m	Left fracture width/mm	Right fracture length/m	Right fracture width/mm
5	9	24.29	25	10.72
10	19	24.73	24	16.79
15	18	25.45	22	19.42
20	19	24.35	19	20.92

(3) The influence of elastic modulus

Refer to 3.2.1 for rock and fracture parameters. The simulation results are shown in Figs. 16, 17 and Table 6. In the first stage of TFIDF mode, the width of the right fracture increases with the increase of injection time, and the larger the elastic modulus, the smaller the fracture width (Fig. 16(a)). In the third stage of TFIDF mode, as the injection time increases, the width and length of the left fracture gradually increase, and the width of the right fracture also changes, especially at an elasticity modulus of 40 GPa, the fracture width decreases as depicted in Fig. 16(b). In general, the influence of elastic modulus on fracture propagation pattern is the same under the two initiation modes. Nevertheless, in the TFIDT mode, the length of the left fracture is restrained,

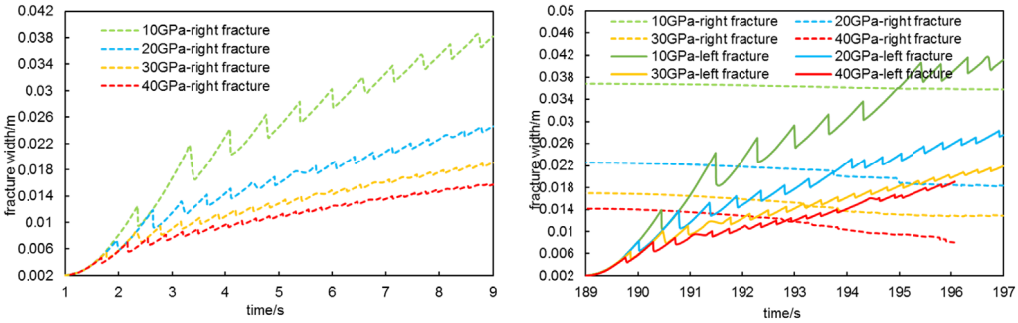

(a) First stage of fracturing (b) The third stage of fracturing

Fig. 16. Fracture width under different elastic modulus in TFIDT mode

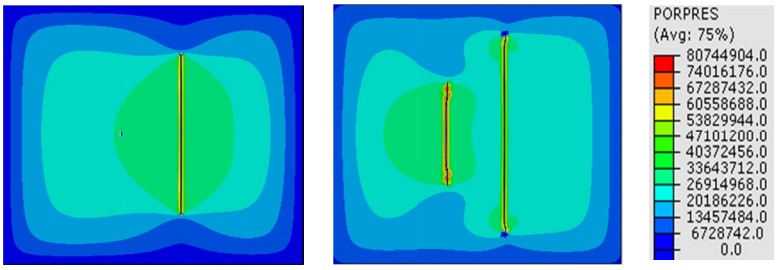

9s 196s

Fig. 17. Pore pressure at different times with an elastic modulus 40 GPa in TFIDT mode

TABLE 6

Fracture length and width under different elastic modulus in TFIDT mode

Elastic modulus /GPa	Left fracture length/m	Left fracture width/mm	Right fracture length/m	Right fracture width/mm
10	11	41.10	12	35.71
20	17	27.43	22	18.34
30	22	21.88	29	12.89
40	29	19.04	32	7.98

while the right fracture is further extended. Compared to the TFIS mode, the difference between the left and right fracture widths of TFIDT mode is greater as the elastic modulus increases, which shows that the influence of the elastic modulus on the fracture propagation pattern remains unchanged, but the influence of the elastic modulus on the fracture propagation pattern will be amplified in the TFIDT mode.

4. Conclusion

TFIS and TFIDT are different fracture initiation modes that may occur in the process of horizontal wells staged fracturing. In this paper, the influences of pumping rate, fracture spacing and elastic modulus on fracture propagation patterns are discussed. The conclusions are as follows:

(1) Increasing the pumping rate will promote the propagation of the fracture. In TFIS mode, two fractures extend alternately under the action of fracture interference. In TFIDT mode, when the pumping rate is greater than 6 m^3/min, a subsequent fracture will affect the expansion of the previously created fracture, and an increase in pumping rate will have a greater impact on the two fractures.

(2) With the increase of fracture spacing, interference between fractures is weakened. In TFIS mode, when the fracture spacing is 5 m, the stress interference between the two fractures intensifies. The fracture then deviates from the direction of the initial maximum principal stress, which is called “mutually repulsive”. In TFIDT mode, as the subsequent fractures expand, the previous fractures are squeezed, the fractures near wellbores are partially closed, the fracture width decreases, the fracture length increases, and the subsequent fractures become shorter and wider. When the fracture spacing is large, the previous fracture is wider. When the fracture spacing is smaller, the previous fracture is longer and narrower, and the two fractures present “inter-attracting”.

(3) When the elastic modulus is small, a short and wide fracture is formed; when the elastic modulus is large, a long and narrow fracture is formed. In TFIS mode, when the elastic modulus is greater than 20 GPa, the left and right fractures expand alternately. In TFIDT mode, the previous and subsequent fractures affect each other. The greater the elastic modulus, the greater the difference between the left and right fracture widths, which amplifies the influence of the elastic modulus on the fracture propagation geometry.

Acknowledgments

This work is supported by Fund project: National Natural Science Foundation of China (51804078, 52074087); China Postdoctoral Science Foundation (2019M651255); Postdoctoral Foundation of Hei Long Jiang (LBH-Z18039)

References

[1] B.X. Huang, X.L. Zhao, J. Ma, T.Y.A. Sun, Field experiment of destress hydraulic fracturing for controlling the large deformation of the dynamic pressure entry heading adjacent to the advancing longwall face. Arch. Min. Sci. **64** (4), 829-848 (2019). DOI: https://doi.org/10.24425/ams.2019.131069

[2] B.W. Xia, L. Liu, Z.Y. Peng, Y.G. Gao, Multi-fracture propagation and deflection laws of horizontal wells in tight sandstone. Chin. J. Geotech. Eng. **42** (8), 1549-1556 (2020). DOI: https://doi.org/10.11779/CJGE202008021

[3] D. Rossana, M. Rinaldi, T. Marco, T. Francesco, Theoretical and computational investigation of the fracturing behavior of anisotropic geomaterials. (2022). DOI: https://doi.org/10.1007/s00161-022-01141-4

[4] D.J. Youn, D.V. Griffiths, Stochastic analysis of hydraulic fracture propagation using the extended finite element method and random field theory. ISRM Regional Symposium – 8th South American Congress on Rock Mechanics. Buenos Aires, Argentina, 15-18 November, ISRM-SCRM-2015-029 (2015).

[5] F.T. Wang, D.L. Shao, C. Zhang, C.K. Zhang, Z.Y. Song, Overlying sand-inrushing mechanism and associated control technology for longwall mining in shallow buried coal seams with the soft surrounding rock. Arch. Min. Sci. **67** (4), 681-697 (2022). DOI: https://doi.org/10.24425/ams.2022.143681

[6] J. Sepehri, M.Y. Soliman, S.M. Morse, Application of extended finite element method to simulate hydraulic fracture propagation from oriented perforations. SPE Hydraul. Fract. Technol. Conf. Texas, USA, 3-5 February, SPE-173342 (2015).

[7] J.J. Sheng, Evaluation of EOR potential of energized fluid fracturing – From an energy perspective. Fuel **307**, 121856 (2022). DOI: https://doi.org/10.1016/j.fuel.2021.121856

[8] K. Wu, J.E. Olson, Mechanisms of Simultaneous Hydraulic-Fracture Propagation From Multiple Perforation Clusters in Horizontal Wells. SPE Journal **21** (3), 1000-1008 (2016). DOI: https://doi.org/10.2118/178925-PA

[9] M. Haddad, K. Sepehrnoori, XFEM-Based CZM for the simulation of 3D multiple-stage hydraulic fracturing in quasi-brittle shale formations. Rock Mech. **49**, 4731-4748 (2015). DOI: https://doi.org/10.1007/s00603-016-1057-2

[10] M. Wang, Z.Q. Guo, C.X. Jiao, S.F. Lu, J.B. Li, H.T. Xue, J.J. Li, J.Q. Li, G.H. Chen, Exploration progress and geochemical features of lacustrine shale oils in China. J. Petrol. Sci. Eng. **178**, 975-986 (2019). DOI: https://doi.org/10.1016/j.petrol.2019.04.029

[11] M.L. Benzeggagh, M. Kenane, Measurement of mixed-mode delamination fracture toughness of unidirectional glass/epoxy composites with mixed-mode bending apparatus. Compos. Sci. Technol. **56** (4), 439-449 (1996). DOI: https://doi.org/10.1016/0266-3538(96)00005-x

[12] Q. Lei, Y. Xu, B. Cai, B.S. Guan, X. Wang, G.Q. Bi, H. Li, S. Li, B. Ding, H.F. Fu, Z. Tong, T. Li, H.Y. Zhang, Progress and prospects of horizontal well fracturing technology for shale oil and gas reservoirs. Petrol. Explor. Dev. **49** (1), 191-199 (2022). DOI: https://doi.org/10.1016/S1876-3804(22)60015-6

[13] Q. Wang, Y. Hu, J. Zhao, L. Ren, A numerical model to simulate fracture network induced by hydraulic fracturing for 3D shale gas reservoir with geo-stress interference. J. Eng. Res-Kuwait. **8** (2), 45-65 (2019).

[14] Q.D. Zeng, J. Yao, Numerical simulation of shale hydraulic fracturing based on the extended finite element method. Appl. Math. Mech. **35** (11), 1239-1248 (2014). DOI: https://doi.org/10.3879/j.issn.10000887.2014.11.007

[15] R. Dimitri, M. Rinaldi, T. Marco, F. Tornabene, F. Corrado, FEM/XFEM modeling of the 3D fracturing process in transversely isotropic geomaterials. Compos. Struct. **276**, 114502 (2021). DOI: https://doi.org/10.1016/j.compstruct.2021.114502

[16] S. Kumar, F. Zhou, K.H. Searles, S.V. Gosavi, Modeling of fluid-driven fractures using XFEM.51st U.S. Rock Mechanics/Geomechanics Symposium. San Francisco, California, USA, 25-28, June, ARMA-2017-0911 (2017).

[17] S. Sun, S. Liang, Y.K. Liu, D. Liu, M.Y. Gao, Y. Tian, J.K. Wang, A Review on Shale Oil and Gas Characteristics and Molecular Dynamics Simulation for the Fluid Behavior in Shale Pore. J. Mol. Liq. **376**, 121507 (2023). DOI: https://doi.org/10.1016/j.molliq.2023.121507

[18] T. Zhou, H.B. Wang, F.X. Li, Y.Z. Li, Y.S. Zou, C. Zhang, Numerical simulation of hydraulic fracture propagation in laminated shale reservoirs. Adv. Pet. Explor. Dev. **47** (5), 1039-1051 (2020). DOI: https://doi.org/10.11698/PED.2020.05.18

[19] T. Zhou, M. Chen, S.C. Zhang, Y.Z. Li, F.X. Li, C. Zhang, Simulation of fracture propagation and optimization of ball-sealer in-stage diversion under the effect of heterogeneous stress field. Nat. Gas Ind. **40** (03), 82-91 (2020). DOI: https://doi.org/10.1016/j.ngib.2020.09.010

[20] T.K. Guo, S.C. Zhang, Y.S. Zou, Numerical simulation of hydraulic fracture propagation in shale gas reservoir. J. Nat. Gas. Sci. Eng. **26**, 847-856 (2015). DOI: https://doi.org/10.1016/j.jngse.2015.07.024

[21] W. Tian, P.C. Li, Y. Dong, Z.W Lu, D.T. Lu, Numerical simulation of sequential, alternate and modified zipper hydraulic fracturing in horizontal wells using XFEM. J. Petrol. Sci. Eng. **183**, 106251 (2019). DOI: https://doi.org/10.1016/j.petrol.2019.106251

[22] W.H. Wang, K. Wu, J. Olson, Characterization of hydraulic fracture geometry in shale rocks through physical modeling. Int. J. Fracture **216** (1), 71-85 (2019). DOI: https://doi.org/10.1007/s10704-019-00343-3

[23] X.L. Wang, F. Shi, H. Liu, H.A. Wu, Numerical simulation of hydraulic fracturing in orthotropic formation based on the extended finite element method. J. Nat. Gas. sci. Eng. **33**, 56-69 (2016). DOI: https://doi.org/10.1016/j.jngse.2016.05.001

[24] X.S. Shang, Y.H. Ding, L.F. Yang, Y.J. Lu, X.M. Yan, Y.H. Wang, Network fracturing technique in shale reservoirs based on weak discontinuity and fracture interaction. Nat. Gas Geosci. **27** (10), 1883-1891 (2016). DOI: https://doi.org/10.11764/j.issn.1672-1926.2016.10.188

[25] Y.K. Zhang, S.B. Chen, X.Y. Li, H.J. Wang, Hydraulic fracturing simulation technology of shale gas reservoir and application of extended finite element method. Nat. Gas Geosci. **32** (1), 109-118 (2021). DOI: https://doi.org/10.11764/j.issn.1672-1926.2020.11.006

[26] Y.M. Song, H. Ren, H.L. Xu, D. An, Experimental study on deformation and damage evolution of a mining roadway with weak layer rock under compression-shear load. Arch. Min. Sci. **66** (3), 351-368 (2022). DOI: https://doi.org/10.24425/ams.2021.138593

[27] Z.R. Chen, Implementation of the extended finite element method for hydraulic fracture problems. 13th International Conference on Fracture, Beijing, China, 16-21 June, 725-739 (2013).